

FEDSM-ICNMM2010-1000,

## MITIGATING BLOCKAGE EFFECTS ON FLOW OVER A CIRCULAR CYLINDER IN AN ADAPTIVE-WALL WIND TUNNEL

**Michael Bishop**

Mechanical and Mechatronics Engineering,  
University of Waterloo,  
Waterloo, Ontario, Canada

**Serhiy Yarusevych**

Mechanical and Mechatronics Engineering,  
University of Waterloo,  
Waterloo, Ontario, Canada

### ABSTRACT

The effect of wall streamlining on flow development over a circular cylinder was investigated experimentally in an adaptive-wall wind tunnel. Experiments were carried out for a Reynolds number of 57,000 and three blockage ratios of 5%, 8%, and 17%. Three test section wall configurations were investigated, namely, geometrically straight walls (GSW), aerodynamically straight walls (ASW), and streamlined walls (SLW). The results show that solid blockage effects are clearly evident in cylinder surface pressure distributions for the GSW and ASW configurations, manifested by an increased peak suction and base suction. Upon streamlining the walls, pressure distributions for each blockage ratio investigated closely match distributions expected for low blockage ratios. Wake blockage limits wake growth in the GSW configuration at 7.75 and 15 diameters downstream of the cylinder for blockages of 17% and 8%, respectively. This adverse effect can be rectified by streamlining the walls, with the resulting wake width development matching that expected for low blockage ratios. Wake vortex shedding frequency and shear layer instability frequency increase in the GSW and ASW configurations with increasing blockage ratio. The observed invariance of the near wake width with wall configuration suggests that the frequency increase is caused by the increased velocity due to solid blockage effects. For all the blockage ratios investigated, this increase is rectified in the SLW configuration, with the resulting Strouhal numbers of about 0.19 matching that expected for low blockage ratios at the corresponding Reynolds number. Blockage effects on the shear layer instability frequency are also successfully mitigated by streamlining the walls.

### INTRODUCTION

Fluid mechanics research and development of relevant engineering applications rely extensively on experimental

testing. Although a variety of facilities is employed, most of experimental facilities have impermeable, rigid test sections, e.g., a closed test section of a wind tunnel. The presence of test section walls is known to give rise to blockage or wall interference effects, which affect experimental data. Three main types of blockage can be classified as solid blockage, wake blockage, and wall boundary layer blockage, e.g., [1-2]. The solid blockage unavoidably occurs when a model is mounted in a closed test section. The flow development is being altered in the confined regions between the model and the test section boundaries, affecting surface stresses on the model and, consequently, forces and moments. The wake blockage and wall boundary layer blockage are attributed to wall interference with model wake development and to the boundary layer growth on test section boundaries, respectively. Both of these types of blockage result in an increase of flow velocity outside of the wake, giving rise to so called horizontal buoyancy [1].

When experimental tests are conducted in the confines of an experimental facility, blockage effects on experimental data have to be accounted for. Several post-test data correction methods have been developed for streamlined and bluff objects, e.g., [2]. Such methods are usually difficult to implement, and their use is typically limited to blockages of less than about 15% [1]. For instance, the results of West & Apelt [3] suggest that common blockage correction methods cannot adequately correct measured pressure distributions on a circular cylinder for blockage ratios greater than 6%. In light of this, to minimize blockage, the size of experimental models is commonly kept small relative to the test section dimensions. This approach, however, limits the effective range of Reynolds numbers achievable in a given facility.

An alternative method aimed at minimizing blockage effects involves building facilities with specialized test sections, where flow at the test section boundaries can be manipulated so as to imitate the conditions in an unbounded

flow. Examples of such facilities are wind tunnels that incorporate ventilated test sections or adaptive-wall test sections, reviewed in detail by Wolf [4] and Meyer & Nitsche [5].

The current investigation focuses on mitigating blockage effects in two-dimensional flows utilizing an adaptive-wall wind tunnel. In adaptive-wall wind tunnels, flexible test section walls are shaped to mimic streamlines of an unbounded flow, with the underlying physical principles of wall streamlining discussed in detail in [4-6]. Wall streamlining is an iterative procedure that relies on experimentally measured pressure distributions along flexible test section walls and the shape of the walls. Several implementation strategies have been developed over the years [4-5]. For two-dimensional testing, the strategies outlined by Wolf & Goodyer [7] and Evenhart [8] are commonly used and have been shown to give comparable results [9].

The majority of previous investigations involving two-dimensional flows in adaptive-wall wind tunnels have been performed on airfoils [4-9]. These investigations focused on reducing blockage effects on aerodynamic forces and moments and demonstrated that such effects can be effectively minimized or virtually eliminated in adaptive-wall tunnels for various airfoil shapes and a range of blockage ratios. In contrast to studies performed on airfoils, there have been a limited number of investigations focused on the effect of wall adaptation on flows over bluff bodies. Recently, Goodyer & Saquib [10] investigated the upper-limit of blockage ratio for which the pressure drag and the Strouhal number can be adequately predicted for a circular cylinder in an adaptive-wall wind tunnel. Tests were conducted for  $Re_d = 52,000$  and model blockage ratios ranging from 20% to 100%. Measurements were limited to characterizing the effect of wall adaptation on mean surface pressure distributions and shedding frequencies. Upon streamlining the walls, adequate estimates of the pressure drag and the Strouhal number were achieved at model blockage ratios of up to 50% and 85%, respectively. Kankainen et al. [11] investigated a circular cylinder in a supercritical regime at a blockage ratio of 30% and  $Re_d = 500,000$ . Their results show that streamlining test section walls eliminates solid blockage effects from the surface pressure distribution.

The present study is motivated by the need for an improved understanding of the effect of wall adaptation on the overall flow development over a given test model. The investigation is focused on the effect of wall adaptation on flow over a circular cylinder, including wake development. The choice of geometry is attributed to the fact that blockage effects on flow development over a circular cylinder have been investigated in several studies performed in fixed-wall wind tunnels, e.g., [3, 12-16]. Providing a comparison baseline for the present work, the results of these studies show that blockage acts to increase drag and vortex shedding frequency and limits wake growth. This investigation was conducted for a Reynolds number of 57,000 and blockages up to 17%, with

wall streamlining performed using the wall adjustment strategy of Wolf & Goodyer [7].

## EXPERIMENTAL SETUP

All measurements were conducted in an adaptive-wall wind tunnel at the University of Waterloo. In this open-return, suction-type tunnel, free-stream velocity can be varied between 3-40 m/s, with a background turbulence intensity of less than 0.3%. The free-stream velocity ( $U_\infty$ ) was set by measuring the pressure drop across the wind tunnel contraction, which was calibrated against a Pitot-static tube positioned in an empty test section at the model location. The uncertainty of the free-stream speed measurements was estimated to be less than 2.5%.

The wind tunnel has a 6 m long test section, comprised of rigid vertical side walls and flexible top and bottom walls. The nominal cross-section of the test section has a height of 0.89 m and a width of 0.61 m. Flexible walls are made of lexan polycarbonate plastic sheets, spanning the entire length of the test section. The shape of each flexible wall can be adjusted by a total of 48 rack and pinions, which are more densely spaced in the vicinity of the model location to allow for a more refined adjustment. The rack and pinions can position the walls to within 0.1 mm of the desired location.

To enable pressure measurements essential for wall adaptation, the flexible top and bottom walls of the test section are equipped with 70 pressure taps each. The taps are placed along the spanwise centre plane of each wall and are more densely spaced near the model location. Wall pressure distributions were acquired via two Scanivalve electronic pressure scanner modules (ZOC33). Pressure transducers in the two modules were calibrated using a GE Precision Portable Pressure Calibrator DPI 610, with the uncertainty associated with wall pressure measurements estimated to be within about  $\pm 0.02$  for  $C_{pw}$  data.

Two plastic circular cylinders, 0.043 m and 0.089 m in diameter, were tested. Both cylinders, centered in the test section, spanned the width of the test section. To allow surface pressure measurements, each cylinder was equipped with a single 0.8 mm diameter pressure tap drilled at its midspan. The pressure tap of the large cylinder was connected directly to a miniature fast-response pressure transducer. Embedding a pressure sensor inside the cylinder allowed for time-resolved pressure measurements. Due to space constraints, the pressure tap of the small cylinder was connected to an external pressure transducer. The uncertainty associated with surface pressure measurements was estimated to be within  $\pm 0.02$  for  $C_p$  data. Surface pressure distributions were acquired by rotating the cylinder using a model-support mechanism, providing an angular resolution of  $0.1^\circ$ . The coordinate system used for data presentation is shown in Fig. 1.

Velocity measurements were performed using a constant temperature anemometry system. A normal hot-wire probe and a cross-wire probe were employed. The probes were positioned in the test section using an automated traversing mechanism with a spatial resolution of  $\pm 0.1$  mm. Using the results of

Kawall et al. (1983), the uncertainties associated with hot-wire velocity measurements were estimated to be less than 5.5%.

To determine the frequency of von Karman vortex shedding and the instability frequency in the separated shear layer, spectral analysis of velocity data was performed. Each spectrum was normalized by the variance of the corresponding signal, so that the area under the spectral curve was unity. The frequency resolution bandwidth of the spectral analysis was 0.3 Hz, sufficient to resolve narrow peaks associated with flow development in the cylinder wake.

## NOMENCLATURE

AR	aspect ratio
ASW	aerodynamically straight walls
B	model blockage ratio
$C_p$	model surface pressure coefficient
$C_{pw}$	wall surface pressure coefficient
d	cylinder diameter
$E_{uu}$	normalized energy spectrum of u
$E_{vv}$	normalized energy spectrum of v
$f_v$	vortex shedding frequency
$f_{sl}$	shear layer instability frequency
GSW	geometrically straight walls
h	vertical height of the test section with GSW
$Re_d$	Reynolds number based on cylinder diameter
RMS	Root Mean Square
St	Strouhal number based on $f_v$
SLW	streamlined walls
$U_o$	free-stream velocity in x direction
$U_o^*$	streamwise velocity at edge of wake
u	streamwise fluctuating velocity component
v	vertical fluctuating velocity component
x, y	streamwise and vertical coordinates, respectively
$\theta$	angle measured from stagnation point on the cylinder

## WALL CONFIGURATIONS

In order to investigate a range of blockage ratios, experiments were conducted in the nominal test section (0.89 m x 0.61 m) and a contracted test section (0.53 m x 0.61 m), with the latter utilized to achieve higher blockage ratios. Table 1 details the test cases investigated. Except for the contraction and diffuser in the contracted test section, the upper and lower flexible walls are spaced by a fixed vertical distance (h) for the entire length of the test section. In this configuration, the walls are referred to as ‘Geometrically Straight Walls’ (GSW). For convenience, the investigated blockage ratios listed in Table 1 will be henceforth rounded to 5%, 8%, and 17%.

TABLE 1. TEST CASES.

Cross- section	h, m	d, m	AR	B, %
0.89 m x 0.61 m	0.890	0.043	14	4.7
0.53 m x 0.61 m	0.527	0.043	14	8.0
0.53 m x 0.61 m	0.527	0.089	7	16.9

In the GSW configuration, the boundary layer growth on the test section walls gives rise to a negative pressure gradient and an increase in streamwise velocity within the test section (Fig. 2). This type of blockage effect was removed in an empty test section by adjusting the flexible walls so as to achieve a zero pressure gradient in the test section. The required wall adjustment was determined based on the expected boundary layer displacement thickness, assuming turbulent boundary layer over the entire test section length, and an empirical correction factor accounting for boundary layer growth on fixed side walls. The resulting wall configuration is referred to as ‘Aerodynamically Straight Walls’ (ASW). Figure 2 depicts wall pressure distributions corresponding to the GSW and ASW configurations measured in an empty test section. The results show that, within the experimental uncertainty, a zero pressure coefficient is attained over the length of the test section in the ASW configuration.

Wall streamlining was implemented using a wall adjustment strategy outlined in detail in [7]. The shape of the flexible walls was adjusted iteratively until the measured pressure distribution on each flexible wall matched that observed in an inviscid flow along a streamline shaped as the corresponding wall. The wall adjustment was implemented with the cylinder installed in the test section and flexible walls set to the ASW configurations. The converged wall configurations for all blockage ratio investigated are referred to as Streamlined Walls (SLW).

## RESULTS

All experiments were conducted for  $Re_d \approx 5.7 \times 10^4$ . To investigate the effect of wall adaptation on the flow development over the circular cylinder model, surface pressure measurements and wake velocity measurements were carried out in the GSW, ASW, and SLW configurations for all the blockage ratios tested.

Figures 3a-c show mean surface pressure distributions for blockages of 17%, 8%, and 5%, respectively. Agreeing with the findings of [14], the results pertaining to the GSW configurations suggest that both the pressure coefficient at the suction peak and the base pressure coefficient decrease with increasing blockage. At a given blockage ratio, the pressure distributions are progressively shifted to higher values by setting the walls into ASW and SLW configurations. When the walls are streamlined, more significant changes in the pressure distributions are observed at higher blockage ratios. In the SLW configuration, the base pressure for all blockage ratios investigated approaches the expected base pressure coefficient of -1.29 observed in low blockage studies at the corresponding Reynolds number [18].

It is of interest to investigate the effect of wall adaptation on the mean separation angle. The separation angle can be estimated based on the location of an inflection point on the surface pressure distribution curve downstream of the suction peak. Based on an analysis of surface pressure measurements, it was established that the separation angle is about  $76^\circ$  (cf.  $77^\circ$  in

[19]) and does not change appreciably with changing the wall configuration or the blockage ratio. This is in agreement with Hiwada & Mabuchi [14], who observed very minor increase in the separation angle with the blockage ratio, which was virtually indiscernible at the blockage ratios comparable to those investigated here. Time-resolved surface pressure measurements conducted for B=17%, not presented here for brevity, also confirmed that the angular position of a peak in the rms pressure fluctuations, linked to the separation location, did not change in the three wall configurations investigated.

Figure 4 shows the pressure distributions measured in the SLW configuration for blockages of 5%, 8% and 17%. In addition, results from [12] obtained at  $Re_d = 32,200$ ,  $B=4.2\%$  and  $AR = 24$  are shown for comparison. The results pertaining to B=5% and 8% overlap, with the relative difference between data points at any angular location being within the experimental uncertainty. The data for these two blockage ratios are also in good agreement with the results from Ref. [12], with minor discrepancies attributable to the differences in test conditions. However, it can be seen in Fig. 4 that the pressure distribution measured in the SLW configuration for B=17% is slightly lower than that measured for B=8% and B=5%. Inherent to studies involving investigations of blockage effects in a given facility, this discrepancy is likely attributed to changes in model aspect ratio (AR). Specifically, a cylinder with  $AR = 14$  was used for B=5% and B=8%, while a larger diameter cylinder ( $AR = 7$ ) was used for B=17% (Table 1). West & Apelt [3] show that decreasing the aspect ratio lowers the pressure distribution, suggesting that the observed discrepancies in data (Fig. 4) are linked to the decrease of the cylinder aspect ratio for B=17%. It is for this reason the present investigation was limited to  $B \leq 17\%$ , since it is usually not feasible to accommodate higher blockage ratios due to the minimum requirements related to model aspect ratio in most experimental studies. Based on the analysis of the results presented in Fig. 4, it can be concluded that the adaptive-wall strategy effectively minimizes blockage effects in surface pressure distributions when all other influencing parameters are held constant.

To investigate mean wake development, cylinder wake was traversed with hot-wire sensors, and wake velocity profiles were acquired at multiple downstream locations. Given the small effects of blockage observed in the pressure distributions for B=5% between the ASW and SLW configurations, velocity profiles in the ASW configuration for B=5% were not obtained. Figure 5 shows the streamwise variation of the mean half wake width (b) for B=5%. The results suggest that the wake growth is not being affected significantly by the change of the wall configuration. A power law fit to the data pertaining to the SLW configuration, shown by a solid line in Fig. 5, gives

$$\frac{b}{d} = 0.67 \left( \frac{x}{d} \right)^{0.51}$$

This suggests that, for B=5%, the wake growth closely follows the  $b \sim x^{0.5}$  scaling expected for low blockages.

Figures 6 and 7 show the downstream growth of the mean half wake width for B=8% and B=17%, respectively. The power law fit obtained for B=5% in the SLW configuration is also shown in both figures for comparison.

For 8% blockage (Fig. 6), the deviations between mean half wake widths measured in the GSW, ASW, and SLW configurations are within experimental uncertainty for  $x/d \leq 9$ . However, due to wake blockage, the wake growth is limited starting at  $x/d=15$  and  $x/d = 19$  in the GSW and the ASW configuration, respectively. Streamlining the walls results in the wake width development matching that measured for B=5%.

For B=17% (Fig. 7), the results show similar wake width development in GSW, ASW, and SLW configurations for  $x/d < 6.5$ . However, downstream, the mean half wake widths in the GSW and ASW configurations deviate significantly from the curve obtained for B = 5%. This indicates that wake blockage has a prominent influence on the wake development for B = 17%. Upon streamlining the walls, the wake is allowed to grow uninhibited and the growth rate matches that measured for B=5%. Based on these results, it can be concluded that streamlining walls adequately corrects the growth of the wake for streamwise locations of  $x/d \leq 19$  and blockages of up to and including 17%.

Figures 8a-c show spectra ( $E_{vv}$ ) of vertical velocity fluctuations for blockages of 17%, 8%, and 5%, respectively. For all the wall configurations, the velocity spectra display dominant peaks attributable to wake vortex shedding. In addition to the dominant peak centered at the shedding frequency ( $f_v$ ), peaks centered at the first and second harmonics of the shedding frequency appear in each spectrum. The results indicate that, for a given blockage ratio, the shedding frequency is the highest in the GSW configuration and is reduced in the ASW and SLW configurations. The deviation in the shedding frequency between wall configurations becomes more pronounced for higher blockage ratios. Although small, a discernable difference in frequencies pertaining to different wall configurations is observed even for B=5%.

Based on the spectra presented in Fig. 8, the corresponding Strouhal numbers are summarized in Table 2. Consistent with the experimental findings of Hiwada & Mabuchi [14], the results pertaining to the GSW configuration show that the Strouhal number increases as the blockage ratio increases. This increase is slightly mitigated in the ASW configuration. For the streamlined walls, the Strouhal number converges to 0.19 for all blockage ratios. This value is in agreement with data presented in Norberg [19] for low blockage ratios.

**TABLE 2 STROUHAL NUMBERS FOR ALL WALL CONFIGURATIONS AND BLOCKAGE RATIOS INVESTIGATED.**

B [%]	GSW	ASW	SLW
17	0.22	0.21	0.19
8	0.21	0.20	0.19
5	0.20	0.20	0.19

It is interesting to note that, although the near wake width is observed to be invariant between the SLW and GSW

configurations, the Strouhal number decreases in the SLW configuration relative to that in the GSW configuration. Thus, it is speculated that the mechanism responsible for the deviation of vortex shedding frequency is mainly due to the velocity change associated with solid blockage effects, i.e., a higher velocity around the model results in higher shedding frequencies. To explore this further, an alternative velocity scaling for the Strouhal number is investigated using the velocity at the edge of the wake at  $x/d = 2.5$ , where the data for the velocity spectra were obtained. The results are shown in Fig. 9. For comparison, the values of the Strouhal number calculated using the traditional formulation ( $St = f_v d/U_o$ ) are also presented. It can be seen that the new scaling results in Strouhal numbers collapsing to within about 3% of the expected  $St$  value of 0.19. This supports the earlier speculation that the main mechanism responsible for the increase of the Strouhal number in the GSW and ASW configurations is the increase of velocity around the cylinder due to solid blockage. By implementing the wall adaptation strategy, the effects of solid blockage are alleviated, and, thus, the value of  $St$  corresponds to that expected for low blockage ratios.

For the investigated flow regime around a circular cylinder, laminar to turbulent transition occurs in the separated shear layer and is known to be associated with the formation of shear layer vortices, whose time and length scales are smaller compared to those of the wake vortices [20-24]. To investigate the effect of wall adaptation on the frequency of the shear layer vortices, i.e., the shear layer instability frequency ( $f_{sl}$ ), spectral analysis of velocity measurements conducted within the separated shear layer was performed. The obtained spectra are shown in Fig. 10. In addition to the dominant peak at the wake vortex shedding frequency, two broader peaks appear at significantly higher frequencies in each spectrum presented in Fig. 10. These peaks are due to the shear layer instability frequency ( $f_{sl}$ ) and its sub-harmonic ( $0.5f_{sl}$ ), with the latter attributed to vortex pairing in the separated shear layer [23]. A detailed analysis of the spectral results showed that, for a given blockage ratio, the shear layer instability frequency is the highest in the GSW configuration and increases as the blockage ratio is increased.

Figure 11 shows the variation of the normalized shear layer instability frequency ( $f_{sl}/f_v$ ) in the present investigation. Previous studies has shown that  $f_{sl}/f_v \sim Re_d^n$  [20-24], with various values of the exponent reported in the literature. For comparison, estimates of  $f_{sl}/f_v$  based on experimental correlations from [21] and [22] are shown in Fig. 11. Considering the difference between the two estimates obtained using these two correlations, they are in good agreement with the present results.

The data presented in Fig. 11 show that, in a given wall configuration,  $f_{sl}/f_v$  increases with the blockage ratio. However, for a given blockage, wall streamlining does not have a significant effect on  $f_{sl}/f_v$ , with the largest difference between the corresponding data points being about 3%. Evidently, as

both  $f_v$  and  $f_{sl}$  are being reduced when walls are streamlined, the ratio of  $f_{sl}/f_v$  remains relatively constant.

## CONCLUSIONS

The effect of wall adaptation on flow development over a circular cylinder has been investigated experimentally. Experiments were conducted at a Reynolds number of 57,000 for blockage ratios of 5%, 8%, and 17% and three wall configurations.

For all the blockage ratios investigated, the mean surface pressure distribution in the GSW configuration is highlighted by an increased suction peak and increased base suction, relative to those observed in the ASW and SLW configurations. Upon streamlining the walls, the adverse blockage effects in the pressure distributions are removed, with the distributions closely following those obtained in previous studies at low blockage ratios.

Mean wake velocity measurements in the GSW configuration suggest that wake width growth is limited at 15 and 7.75 diameters downstream of the cylinder axis for blockages of 8% and 17%, respectively. Streamlining the walls corrects this limitation and allows the half wake width ( $b$ ) to develop with streamwise distance ( $x$ ) at the rate expected for low blockage ratios (i.e.,  $b \sim x^{0.5}$ ). For  $B=5\%$ , wake width growth is uninhibited in both the GSW and SLW configurations.

The results show that the vortex shedding frequency increases with the blockage ratio. For  $B=17\%$ , the Strouhal number of 0.22 observed in the GSW configuration is reduced to  $St=0.21$  and  $St=0.19$  in the ASW and SLW configurations, respectively. For all the cases investigated, streamlining the walls results in a Strouhal number falling within the range expected for low blockage ratios. The observed invariance of the near wake half width development to blockage effects suggests that the mechanism responsible for the increase in vortex shedding frequency is likely due to the increase of velocity outside of the near wake caused by solid blockage effects. Indeed, normalizing the shedding frequency by the wake edge velocity, as opposed to the free-stream velocity measured upstream of the model, results in the Strouhal numbers collapsing on  $St \approx 0.19$ .

Similar to the vortex shedding frequency, the shear layer instability frequency is the highest in the GSW configuration, being reduced slightly in the ASW configuration and more substantially in the SLW configuration. It is noted that although the shear layer instability frequency increases in the GSW configuration with blockage, the normalized shear layer instability frequency ( $f_{sl}/f_v$ ) does not vary appreciably for a given blockage ratio.

## ACKNOWLEDGMENTS

The authors thankfully acknowledge the Natural Sciences and Engineering Research Council of Canada for funding of this work.

## REFERENCES

- [1] Tavoularis, S., 2005, *Measurement in Fluid Mechanics*, Cambridge University Press, New York, Chapter 6.
- [2] Barlow, J. B., Rae, W. H., Pope, A. 1999, *Low-Speed Wind Tunnel Testing*, John Wiley and Sons, New York, Chapter 9.
- [3] West, G.S., and Apelt, C.J., 1982, "The Effects of Tunnel Blockage and Aspect Ratio on the Mean Flow Past a Circular Cylinder with Reynolds Numbers between  $10^4$  and  $10^5$ ," *Journal of Fluid Mechanics*, **114**, pp. 361-377.
- [4] Wolf, S.W.D., 1995, "Adaptive Wall Technology for Improved Wind Tunnel Testing Techniques – a Review," *Progress in Aerospace Sciences*, **31**, pp. 85-136.
- [5] Meyer, O., and Nitsche, W., 2004, "Update on Progress in Adaptive Wind Tunnel Wall Technology," *Progress in Aerospace Sciences*, **40**, pp. 119-141.
- [6] Sears, W. R., and Erickson, J. C., 1988, "Adaptive Wind Tunnels," *Annual Review of Fluids Mechanics*, **20**, pp. 17-34.
- [7] Wolf, S.W.D., and Goodyer, M.J., 1988, "Predictive Wall Adjustment Strategy for Two-Dimensional Flexible Walled Adaptive Wind Tunnel – a Detailed Description of the First One-Step Method," NASA CR 181635.
- [8] Everhart, J.L., (1983 "A Method for Modifying Two-Dimensional Adaptive Wind Tunnel Walls Including Analytical and Experimental Verification," NASA TP-2081.
- [9] Russo, G.P, Zuppari, G., and Basciani, M., 1995 "An Experimental Comparison of Two Adaptation Strategies in an Adaptive-Walls Wind Tunnel," *Experiments in Fluids*, **19** (4), pp. 274-279.
- [10] Goodyer, M.J., and Saquib, M., 2007, "Blockage Limits in a Two-Dimensional Self-Streamlining Wind Tunnel," *25<sup>th</sup> AIAA Applied Aerodynamics Conference*, AIAA 2007-3818.
- [11] Kankainen, P., Brundrett, E., and Kaiser, J.A., 1994 "A Small Wind Tunnel Significantly Improved by a Multi-Purpose, Two-Flexible-Wall Test Section," *Journal of Fluids Engineering*, Vol. 116, pp. 419-423.
- [12] Okamoto, T., and Takeuchi, M., "Effect of Side Walls of Wind Tunnel on Flow Around Two-Dimensional Circular Cylinder and its Wake," *Bull. JSME*, Vol. 18, 1975, pp. 1011-1017.
- [13] Richter, A. and Naudascher, E., 1976, "Fluctuating Forces on a Rigid Circular Cylinder in Confined Flow," *Journal of Fluid Mechanics*, **78**, pp.561-576.
- [14] Hiwada, M., and Mabuchi, I., "Flow Behaviour and Heat Transfer Around the Circular Cylinder at High Blockage Ratios," *Heat Transfer Jap. Res.*, Vol. 10, 1981, pp.17-39.
- [15] Ramamurthy, A.S., and Lee, P.M., "Effect of Blockage on Steady Force Coefficients," *ASCE J. Engg. Mech. Div.*, Vol. 99, 1973, pp.755-772.
- [16] Zdravkovich, M.M., 2003, "*Flow Around Circular Cylinders Vol 2: Applications*," Oxford University Press, Oxford.
- [17] Kawall, J.G., Shokr, M., and Keffer, J.F., 1983, "A Digital Technique for the Simultaneous Measurements of Streamwise and Lateral Velocities in Turbulent Flows," *Journal of Fluid Mechanics*, **133**, pp. 83-112.
- [18] Roshko, A., 1993 "Perspectives of Bluff Body Aerodynamics," *Journal of Wind Engineering and Industrial Aerodynamics*, **49**, pp.79-100.
- [19] Norberg, C., 2003, "Fluctuating Lift on a Circular Cylinder: Review and New Measurements," *Journal of Fluids and Structures*, **17**, pp. 57-96.
- [20] Bloor, M.S., 1964, "The Transition to Turbulence in the Wake of a Circular Cylinder," *Journal of Fluid Mechanics*, **19**, pp. 290-304.
- [21] Prasad, A., and Williamson, C.H.K., 1997, "The Instability of the Shear Layer Separating from a Bluff Body," *Journal of Fluid Mechanics*, **333**, pp. 375-402.
- [22] Norberg, C., 1987, "Effect of Reynolds Number and a Low-Intensity Freestream Turbulence on the Flow Around a Circular Cylinder," *Publication 87/2*, Dept. Applied Thermodynamics and Fluid Mechanics, Chalmers University of Technology, Gothenburg, Sweden.
- [23] Rajagopalan, S., and Antonia, R.A., 2005, "Flow Around a Circular Cylinder – Structure of the Near Wake Shear Layer," *Experiments in Fluids*, **38**, pp. 393-402.

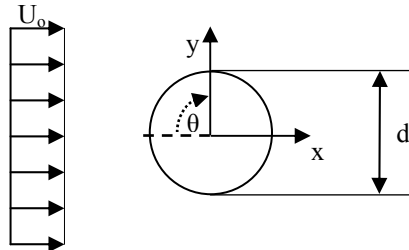


FIG. 1 COORDINATE SYSTEM.

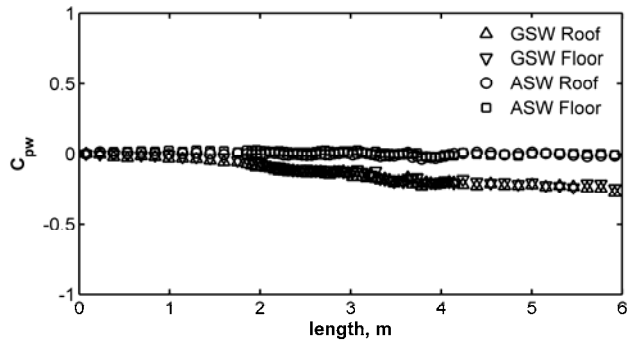


FIG. 2 WALL PRESSURE DISTRIBUTIONS IN AN EMPTY TEST SECTION FOR GSW AND ASW.

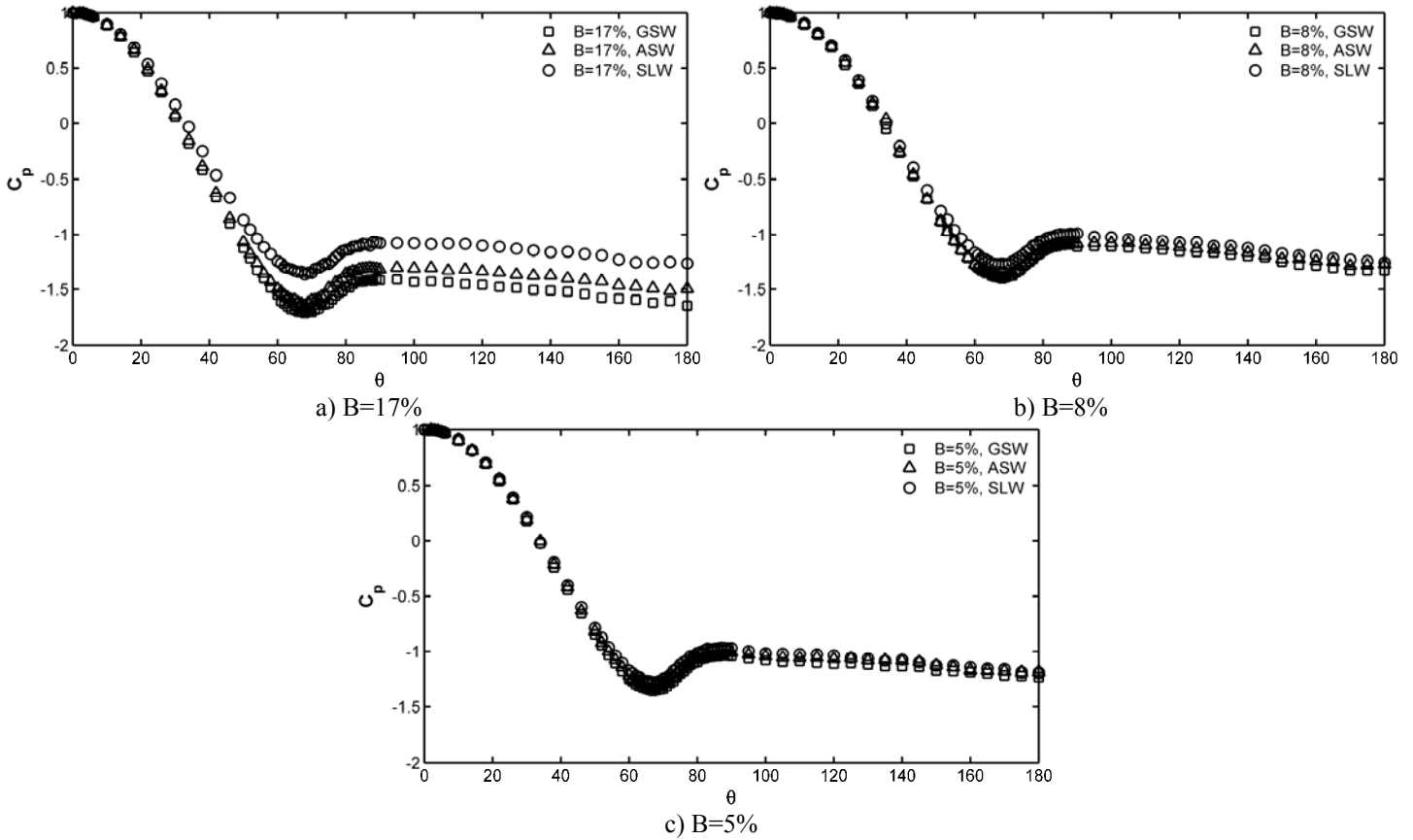


FIG. 3 SURFACE PRESSURE DISTRIBUTIONS IN THE GSW, ASW, AND SLW CONFIGURATIONS.

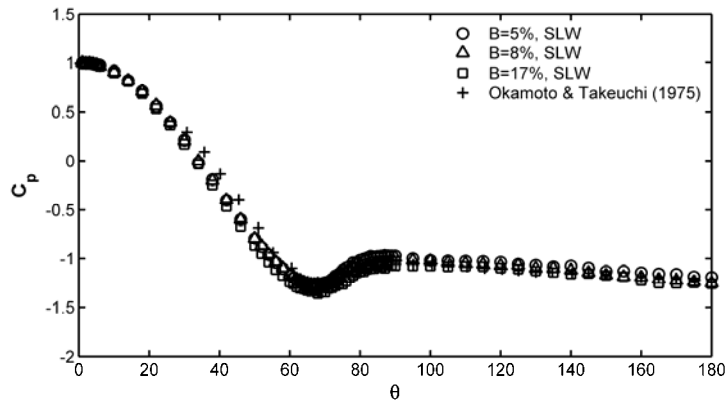


FIG. 4 SURFACE PRESSURE DISTRIBUTIONS IN THE SLW CONFIGURATION. NOTE THE DATA FROM REF. [12] PERTAINS TO  $Re_d = 32,200$  AND  $B=4.2\%$ .

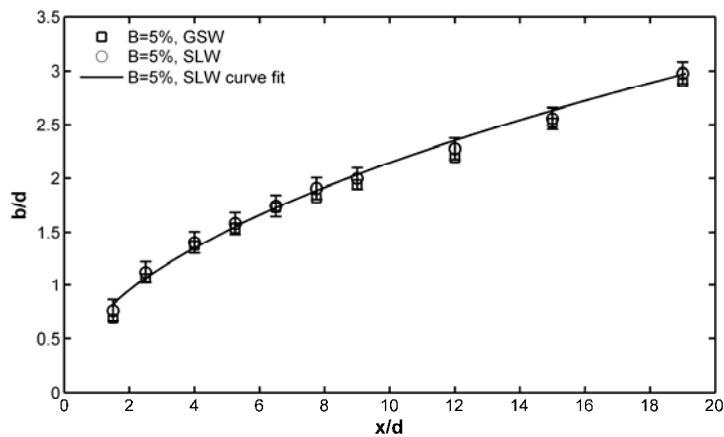


FIG. 5 MEAN HALF WAKE WIDTH GROWTH FOR  $B=5\%$  IN THE GSW AND SLW CONFIGURATIONS.

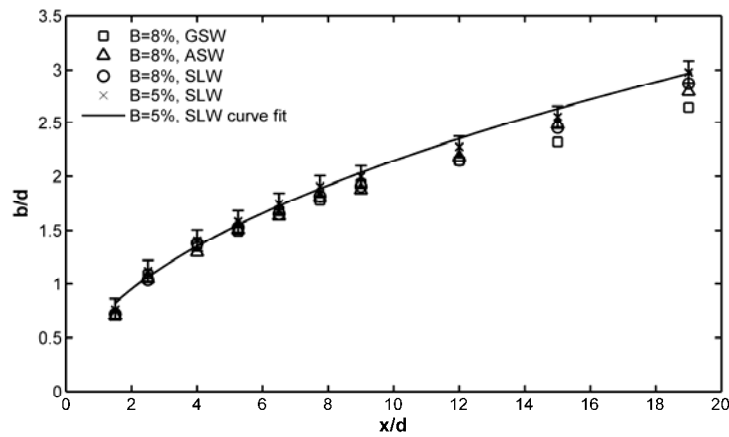


FIG. 6 MEAN HALF WAKE WIDTH GROWTH FOR  $B=8\%$  IN THE GSW, ASW, AND SLW CONFIGURATIONS.

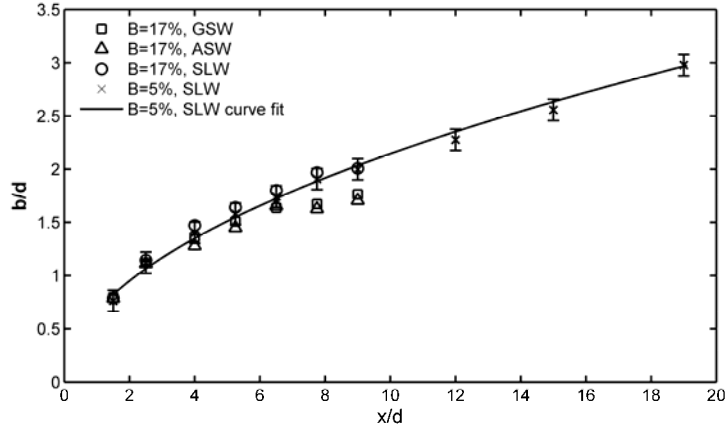


FIG. 7 MEAN HALF WAKE WIDTH GROWTH FOR B=17% IN THE GSW, ASW, AND SLW CONFIGURATIONS.

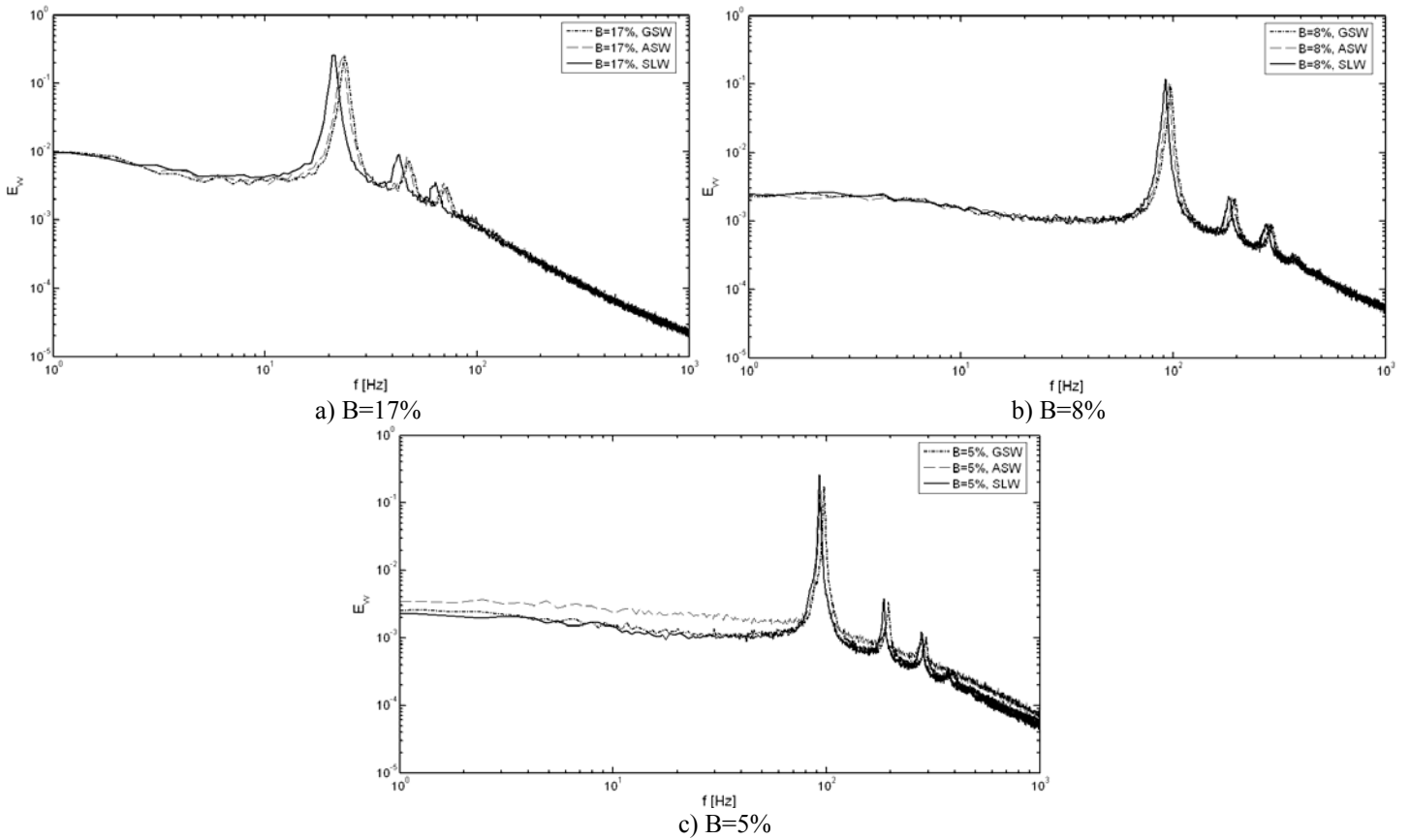


FIG. 8 SPECTRA OF THE VERTICAL FLUCTUATING COMPONENT MEASURED AT X/D=2.5, Y/D=0.5.

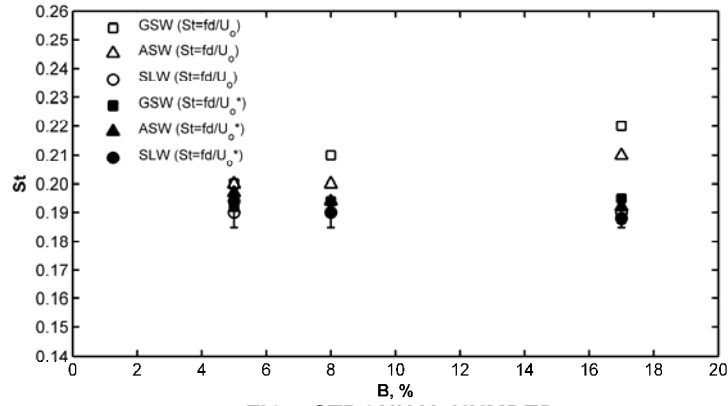


FIG.9 STROUHAL NUMBER.

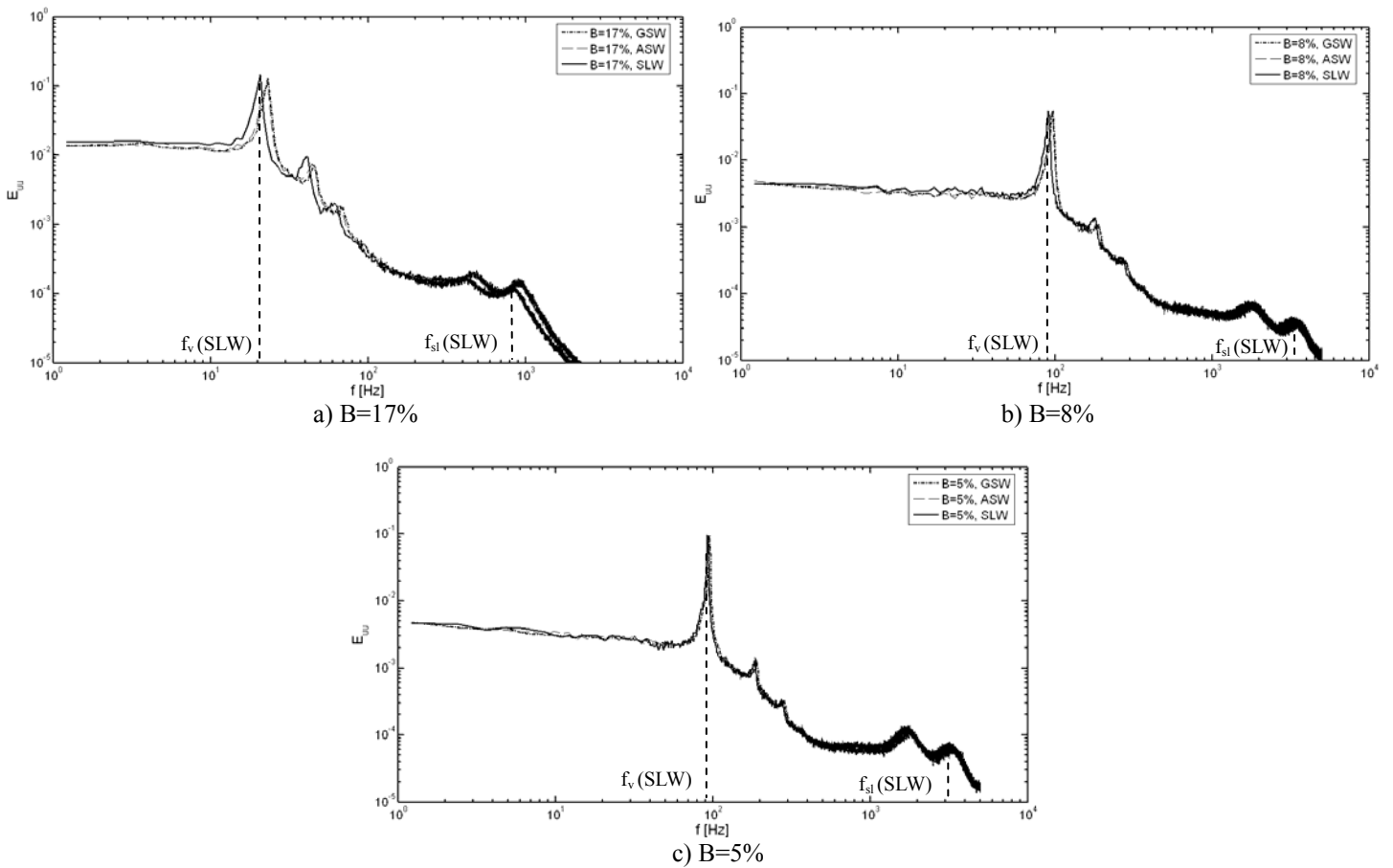


FIG. 10 SPECTRA OF STREAMWISE VELOCITY FLUCTUATIONS MEASURED IN THE SEPARATED SHEAR LAYER AT  $X/D = 0.25$  AND  $Y/D = 0.62$ .

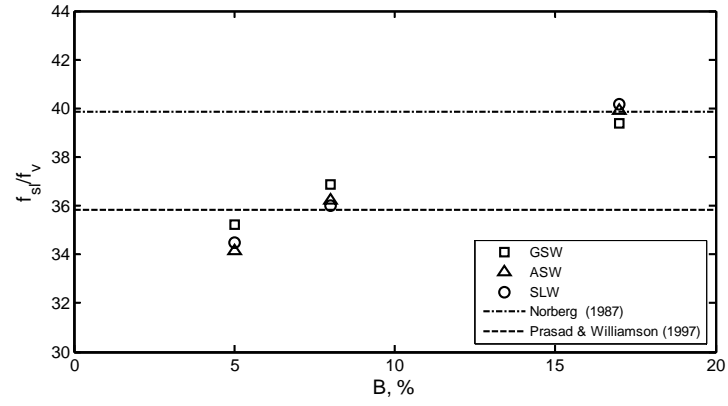


FIG. 11 NORMALIZED SHEAR LAYER INSTABILITY FREQUENCY.